# Intramolecular Charge Transfer in a Star-Shaped Oligoarylamine

**Yasukazu Hirao, Akihiro Ito,* and Kazuyoshi Tanaka†**

*Department of Molecular Engineering, Graduate School of Engineering, Kyoto University, Nishikyo-ku, Kyoto 615-8510, Japan, and CREST, Japan Science and Technology Agency (JST), Japan*

*Received: December 25, 2006; In Final Form: February 7, 2007*

The intervalence (IV) states of the monocationic states of the star-shaped nonaamine (**3**) and the triamine (**2**) as the branched unit in **3** have been examined by electrochemical, spectroelectrochemical, and temperature-dependent ESR spectroscopy. The oligoarylamines **2** and **3** were synthesized by using the successive palladium-catalyzed amination reaction. The redox property of **3** was basically the same as that of **2**. However, there exist small potential differences between the first three one-electron oxidations for **3**, indicating electronic coupling among the peripherally substituted triamine moieties via the central 1,3,5-benzenetriyl bridging unit. The observed ESR spectral pattern for $\mathbf{2}^+$ remained unchanged over the measured temperature range. From the spectral simulation analyses, it was concluded that the unpaired electron in $\mathbf{2}^+$ is fully delocalized over the whole molecule on the ESR time scale. This conclusion was corroborated by comparison of its optical absorption spectrum with TD-DFT-calculated results. In contrast, the peak-to-peak ESR line width ($\Delta H_{PP}$) of $\mathbf{3}^+$ exhibited temperature dependency. This behavior is ascribed to the thermally activated intramolecular charge transfer (ICT) among the branched three triamine moieties via the central 1,3,5-benzenetriyl bridging unit. From the spectral simulations based on the stochastic Liouville method, the first-order rate constant at each temperature and the parameters of the energy barrier for the ICT in $\mathbf{3}^+$ were successfully determined.

## Introduction

In conjunction with the application to the molecular-based electronic and optoelectronic devices, oligoarylamines have attracted considerable interest in recent years.[1,2] Such a trend is closely related to the outstanding development of the studies on the palladium-catalyzed amination reaction[3−5] which makes it possible to synthesize oligoarylamines of various structures.[6−9] In particular, owing to their strong electron-donor properties and their ability to form glassy amorphous phases, "star-shaped" oligoarylamines are considered to be useful for hole-transport (HT) materials in organic electroluminescent devices (OELD).[2] For the exploitation of the efficient HT materials in OELD, much attention has been paid to the intermolecular charge-transfer properties in the molecular glassy state.

On the other hand, extensive studies have so far been made on the nature of the intervalence (IV) states in the oxidized states of oligoarylamines.[8,10−14] In the IV compound, two (or more) equivalent redox-active sites are connected by the proper bridging units, and the valence-mixing takes place in the partially oxidized (or reduced) states. The arylamines can be regarded as useful redox-active units due to the stability of their cationic states. The elucidation of the IV states in organic compounds is essentially important for an understanding of the intramolecular charge-transfer (ICT) process in nanometer-sized molecules such as molecular wires and dendrimers, which can be regarded as promising core units for unimolecular electronic devices.[15]

In the present study, we focused on the IV states in the monocationic state of the star-shaped nonaamine (Chart 1, **3**). The nonaamine **3** contains a 1,3,5-benzenetriyl bridging unit and branched three arylamine units which are connected by the bridging unit. The branched arylamine unit has three redox-active amino groups linked by the *para*-phenylene rings. It is noteworthy that the IV compounds bearing two redox-active amino groups have been extensively examined so far.[10−14] In particular, it is well-known that the *para*-phenylenediamine radical cation ($\mathbf{1}^+$) has the delocalized IV state in which the unpaired electron is fully delocalized over the whole molecule.[13] In addition, it recently developed that chemical modification of the redox-active units or the bridging unit causes a significant effect on the IV states in bis(triarylamine) systems.[8,11,14] On the other hand, little attention has been paid to the IV states in the multi-redox-active site systems including several triarylamine moieties. In this context, the IV state in the branched triamine moiety in **3** is of great interest. The triamine **2** is suitable for an understanding of the IV state within the branched triamine moiety in **3**.

**CHART 1: Linear-Shaped Diamine 1 and Triamine 2 and the Star-Shaped Nonaamine 3**

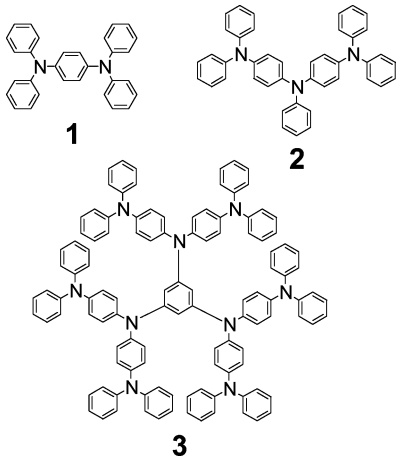


* Corresponding author. E-mail: aito@scl.kyoto-u.ac.jp.
† Japan Science and Technology Agency (JST).

10.1021/jp068917t CCC: $37.00 
Published on Web 03/27/2007

**SCHEME 1: Synthesis of the Triamine 2**

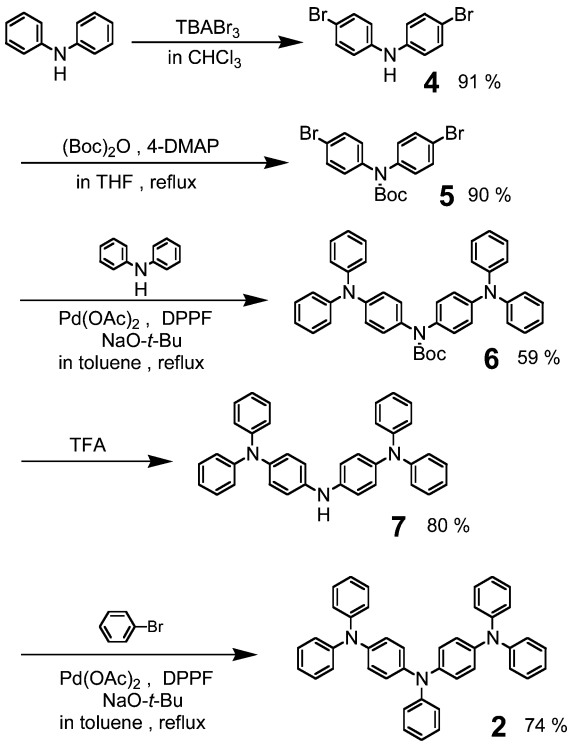


$TBABr_3$=tetra-*n*-butylammonium tribromide
4-DMAP=4-dimethylaminopyridine
DPPF=1,1'-bis(diphenylphosphino)ferrocene
TFA=trifluoroacetic acid

**SCHEME 2: Synthesis of the Star-Shaped Nonaamine 3**

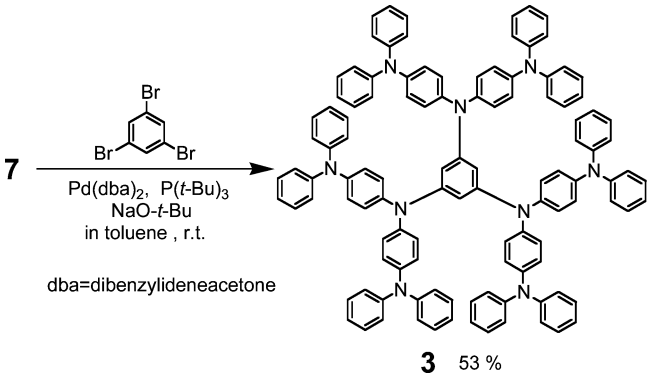


Moreover, the star-shaped oligoarylamines based on the 1,3,5-benzenetriyl framework has three quasi-degenerate nonbonding molecular orbitals (NBMOs), leading to the high-spin ground state for the three-electron oxidized state.[16,17] In fact, our previous work on the derivative of **3** has demonstrated the high-spin preference in its tri(radical cation).[7g] Thus, a similar electronic structure can be expected for **3**. Our concern is to consider how such characteristic molecular and electronic structures of **3** influence the IV state in its oxidized state. Here, we report on the IV states of $\mathbf{2}^+$ and $\mathbf{3}^+$ on the basis of the electrochemical, spectroelectrochemical, and ESR measurements.

## Experimental Section

**Electrochemical Measurements.** Cyclic voltammograms were recorded using an ALS/chi Electrochemical Analyzer model 612A with a three-electrode cell using a Pt disk (2 $mm^2$) as the working electrode, a Pt wire as the counter electrode, and an Ag/0.01 M $AgNO_3$ (MeCN) as the reference electrode calibrated against a ferrocene/ferrocenium ($Fc/Fc^+$) redox couple in a solution of 0.1 M tetra-*n*-butylammonium tetrafluoroborate as a supporting electrolyte (298 K, scan rate 100 $mVs^{-1}$).

**TABLE 1: Redox Potentials (V vs $Fc/Fc^+$) and Potential Differences of 1−3 in Benzonitrile and Dichloromethane at 298 K**

| | $E_1$ | $E_2$ | $E_3$ | $E_4$ | $E_5$ | $E_6$ | $\Delta E_{1-2}$ | $\Delta E_{1-4}$ |
|---|---|---|---|---|---|---|---|---|
| | | | | benzonitrile/ 0.1 M $TBABF_4$ | | | | |
| **1** | 0.14 | 0.59 | | | | | 0.45 | |
| **2** | 0.04 | 0.35 | 1.04[a] | | | | 0.31 | |
| **3** | −0.01 | 0.14 | 0.25 | 0.38[b] | 1.10[a,b] | | 0.15 | 0.39 |
| | | | | dichloromethane/0.1 M $TBABF_4$ | | | | |
| **1** | 0.11 | 0.58 | | | | | 0.45 | |
| **2** | 0.01 | 0.36 | 1.09[a] | | | | 0.35 | |
| **3** | −0.05 | 0.13 | 0.21 | 0.38[b] | 1.17[a,b] | | 0.18 | 0.43 |

[a] Oxidation peak potential (irreversible). [b] Quasi-three-electron oxidation.

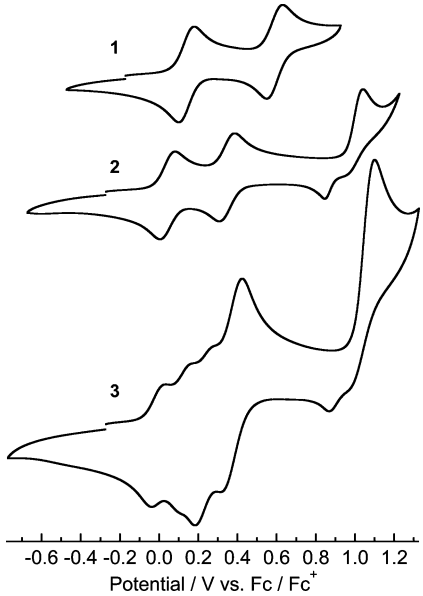


**Figure 1.** Cyclic voltammograms of oligoarylamines **1**, **2**, and **3** in benzonitrile/0.1 M *n*-$Bu_4NBF_4$ at 298 K (scan rate 100 mV $s^{-1}$).

**ESR Measurements.** ESR spectra were measured using a JEOL JES-SRE2X or a JEOL JES-TE200 X-band spectrometer in which temperatures were controlled by a JEOL ES-DVT2 variable-temperature unit or a JEOL ES-DVT3 variable-temperature unit, respectively. The determinations of the *g* values and the hyperfine coupling constants were performed using a $Mn^{2+}$/MgO solid solution as a standard.

**UV/Vis/NIR Spectrum Measurements.** The spectra were measured with a Perkin-Elmer Lambda 19 spectrometer. Spectroelectrochemical measurements were performed using an optically transparent thin-layer electrode quartz cell (light path length = 1 mm). The working and the counter electrodes were a Pt mesh and a Pt coil, respectively. The reference electrode was an Ag wire. The potential was applied with an ALS/chi Electrochemical Analyzer model 612A.

## Results and Discussion

**Synthesis.** The synthesis of the triamine **2**[18] as the branched unit of **3** was carried out by following the procedure shown in Scheme 1. Treatment of diphenylamine with tetrabutylammonium tribromide ($TBABr_3$) gave the dibrominated diphenylamine **4**.[19] After protection of the secondary amino group of **4**

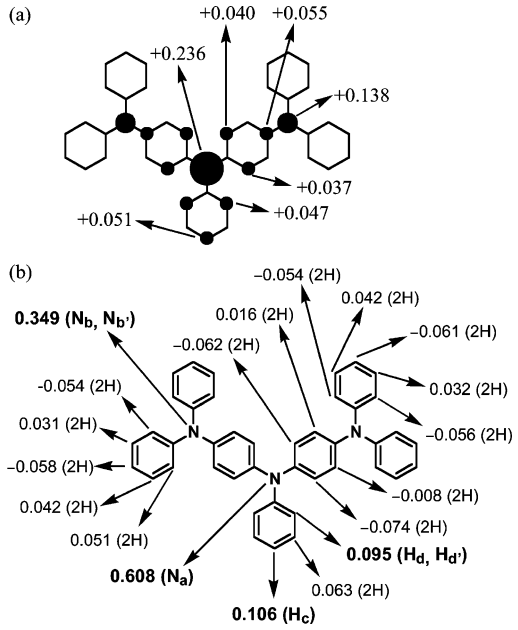


**Figure 2.** (a) Spin density distributions, and (b) $^{1}$H and $^{14}$N hyperfine coupling constants (mT) for $\mathbf{2}^{+}$ ($C_2$ symmetry) at the UB3LYP/3-21G* level of theory.

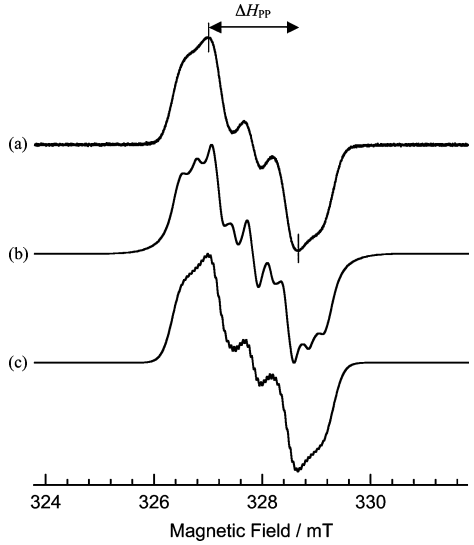


**Figure 3.** (a) Observed ESR spectrum of $\mathbf{2}^{+}$ in DM at 293 K, and the simulated spectra with (b) $a_{N_a} = 0.66$ mT, $a_{N_{b,b'}} = 0.275$ mT, $a_{H_{c,d,d'}} = 0.10$ mT, and the line width = 0.20 mT; (c) $a_{N_a} = 0.66$ mT, $a_{N_{b,b'}} = 0.275$ mT, $a_{H_{c,d,d'}} = 0.10$ mT, $a_{H_{ave}} = 0.05$ mT for the remaining 30 hydrogen nuclei, and line width = 0.08 mT.

with a *tert*-butoxycarbonyl (BOC) group,[6a,b] BOC-protected triamine **6** was prepared by using a palladium-catalyzed amination reaction between the BOC-protected di(4-bromophenyl)amine **5** and diphenylamine in the presence of $Pd(OAc)_2$ and 1,1′-bis(diphenylphosphanyl)ferrocene (DPPF);[3a,4a] moreover, **6** was deprotected to yield triamine **7** with trifluoroacetic acid (TFA).[20] Finally, **2** was obtained by the same palladium-catalyzed amination reaction between triamine **7** and bromobenzene. On the other hand, by the use of $Pd(dba)_2$ and $P(t\text{-}Bu)_3$ as a catalytic system, a palladium-catalyzed amination reaction between 1,3,5-tribromobenzene and triamine **7** afforded the star-shaped nonaamine **3** in 53% yield (Scheme 2).[4d,5,6d] The synthetic details are given in the Supporting Information.

**Electrochemistry.** The redox properties of **2** and **3** were evaluated by cyclic voltammetry (CV) in benzonitrile (BN) solution at 298 K with 0.1 M tetra-*n*-butylammonium tetrafluoroborate as supporting electrolyte. In addition to these two oligoarylamines, *N*,*N*,*N*′,*N*′-tetraphenyl-1,4-benzenediamine (**1**) as a reference compound was also measured under the same conditions. A similar CV response was also observed in

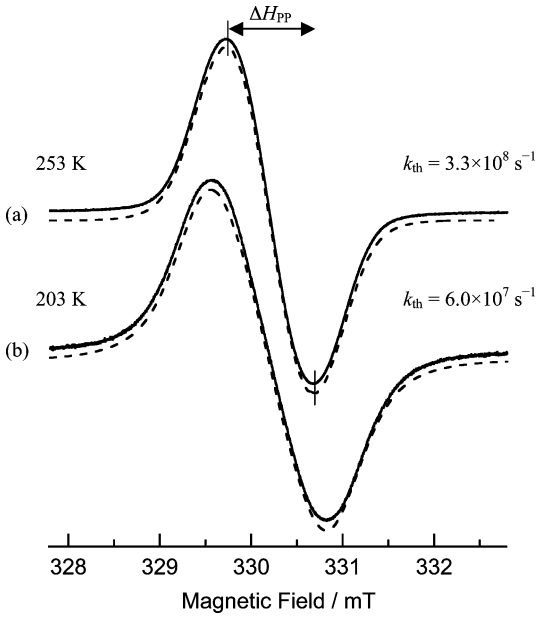


**Figure 4.** Observed ESR spectra for $\mathbf{3}^{+}$ in dichloromethane (solid line) and their simulated spectra (dashed line). (a) $k_{th} = 3.3 \times 10^8$ s$^{-1}$, line width = 0.12 mT, at 253 K; (b) $k_{th} = 6.0 \times 10^7$ s$^{-1}$, line width = 0.15 mT, at 203 K.

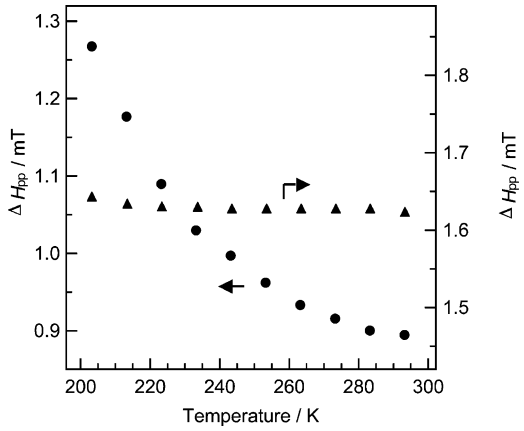


**Figure 5.** Temperature dependence of the peak-to-peak line width $\Delta H_{PP}$ for the ESR spectra of $\mathbf{2}^{+}$ (triangle) and $\mathbf{3}^{+}$ (circle).

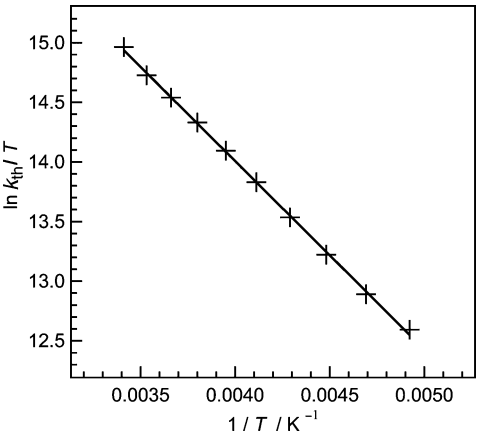


**Figure 6.** Eyring plot of the ICT rate constant ($k_{th}$) for $\mathbf{3}^{+}$ obtained from the ESR spectrum simulations.

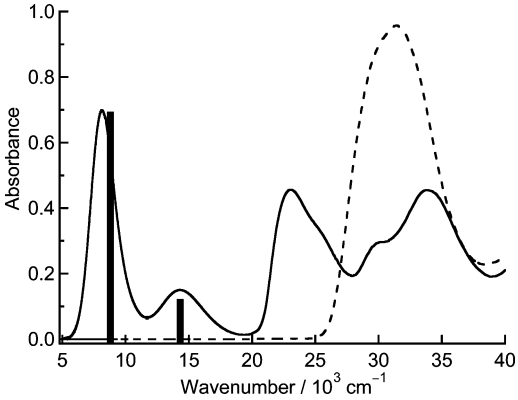


**Figure 7.** UV/vis/NIR spectra for **2** (dashed curve) and $\mathbf{2}^+$ (solid curve) in dichloromethane/0.1 M *n*-$Bu_4NBF_4$. The black sticks represent the calculated lowest and next-lowest transition energies and their oscillator strengths for $\mathbf{2}^+$ ($C_2$ symmetry).

dichloromethane (DM) solution. The results in both BN and DM solutions are summarized in Table 1, together with the potential differences between the first and second oxidation potentials ($\Delta E_{1-2}$) and the first and fourth oxidation potentials ($\Delta E_{1-4}$).

The voltammogram of the triamine **2** showed two reversible oxidation waves and the subsequent irreversible oxidation wave (Figure 1). The first oxidation potential of **2** shifts lower as compared to that of **1**. This suggests that the first oxidation process corresponds to the removal of one electron from the central triphenylamine moiety of **2**. The density functional (DFT) calculations for $\mathbf{2}^+$ supported the concept that the generated unpaired electron is mainly distributed on the central triphenylamine moiety (Figure 2a).[21] Moreover, it is noteworthy that the potential difference $\Delta E_{1-2}$ of 0.31 V for **2** is smaller than 0.45 V for **1**. This result indicates that the electrostatic repulsion in $\mathbf{2}^{2+}$ is reduced as compared to that in $\mathbf{1}^{2+}$.

As shown in Figure 1, the voltammogram of **3** revealed four reversible oxidation waves and the subsequent irreversible oxidation wave. The observed oxidation peak currents for the fourth and the fifth waves were almost three times as large as those for the first three oxidation waves. Moreover, the first, fourth, and fifth oxidation potentials of **3** were roughly identical to the first, second, and third oxidation potentials of **2**, respectively. These results strongly suggest that the redox behavior of **3** can be basically interpreted as the superposition of the oxidation processes originating from each branched triamine moiety. Thus, each of the first three oxidation processes (−0.01 to 0.25 V in BN) can be viewed as the three successive one-electron oxidation processes from the branched three triamine moieties, while the fourth (0.38 V in BN) [and the fifth (1.10 V in BN)] oxidation process in BN corresponds to the simultaneous one-electron oxidation from the three one-electron-oxidized (and the two-electron-oxidized) triamine moieties so as to generate the hexacation $\mathbf{3}^{6+}$ (and the nonacation $\mathbf{3}^{9+}$). It should be noted that the first three one-electron oxidation processes did not occur at the same potential. For instance, the $\Delta E_{1-2}$ for **3** was estimated to be 0.15 V. As discussed in the later section, this clearly shows that we cannot ignore the electronic coupling via the 1,3,5-benzenetriyl bridging unit and suggests the existence of the IV charge-transfer (IV-CT) state in $\mathbf{3}^+$.

**Dynamic ESR Measurements.** The IV states in $\mathbf{2}^+$ and $\mathbf{3}^+$ were studied by temperature-dependent ESR spectroscopy. The radical cations for the measurements were obtained by the chemical oxidation with 0.8 equivalents of tris(4-bromophenyl)-aminium hexachloroantimonate at 195 K in dichloromethane (DM). Both of the generated radical cations, $\mathbf{2}^+$ and $\mathbf{3}^+$, were found to be stable under anaerobic conditions at room temperature. The ESR spectrum of $\mathbf{2}^+$ at room temperature showed a broad five-line pattern (Figure 3a), and the spectral line shape remained unchanged over a wide temperature range from 293 to 203 K. A number of hydrogen nuclei in $\mathbf{2}^+$ having the various hyperfine coupling (hfc) constants result in such a broad line width. The calculated hyperfine coupling constants are shown in Figure 2b. As indicated by the DFT calculations on $\mathbf{2}^+$, it is expected that the major contributions to the hyperfine splitting in the ESR spectrum come from the central nitrogen nucleus ($N_a$), the peripheral two equivalent nitrogen nuclei ($N_b$ and $N_{b'}$), and the three hydrogen nuclei ($H_c$, $H_d$, and $H_{d'}$) at the para and ortho positions of the central *N*-substituted phenyl ring. In contrast, the remaining 30 hydrogen nuclei make relatively small contributions. In fact, the observed ESR spectrum can be roughly simulated with the hfc constants of the above-mentioned five nuclei ($a_{N_a} = 0.66$ mT, $a_{N_{b,b'}} = 0.275$ mT, and $a_{H_{c,d,d'}} = 0.10$ mT) (Figure 3b). In this simulation, the hfc constants for the three hydrogen nuclei were assumed to be approximately the same value, as is supported by the DFT calculations. Moreover, the contributions from the remaining 30 hydrogen nuclei in $\mathbf{2}^+$ were incorporated into the spectral line width as a simulation parameter (line width = 0.20 mT). Alternatively, introducing the average value ($a_{H_{ave}} = 0.05$ mT) of the calculated hfc constants for those 30 hydrogen nuclei instead of incorporating them into the spectral line width, we obtained the best simulated ESR spectrum (Figure 3c). As a result, the ESR spectral pattern of $\mathbf{2}^+$ and its temperature independency lead to the conclusion that the unpaired electron in $\mathbf{2}^+$ is completely delocalized over the whole molecule on the ESR time scale.

**TABLE 2: TD-DFT (UB3LYP/3-21G*) Calculations of the Optical Spectrum for $\mathbf{2}^+$**

| | | TD-DFT calcn | | |
|---|---|---|---|---|
| species | $h\nu$ (obs) ($cm^{-1}$) | $h\nu$ ($cm^{-1}$) ($f$) | assignment | |
| $\mathbf{2}^+$ | 8117 | 8700 (0.56) | 72% | 152$\beta$ → 153$\beta$ |
| | | | 2% | 153α → 154α |
| | 14350 | 14210 (0.11) | 91% | 151$\beta$ → 153$\beta$ |
| | | | 1% | 153α → 156α |
| | | | 1% | 152α → 154α |

In contrast, the ESR spectrum of the star-shaped nonaamine $\mathbf{3}^+$ changes its peak-to-peak width ($\Delta H_{PP}$) according to the temperature change. While $\mathbf{3}^+$ showed only a single broad ESR spectrum over the whole temperature range (Figure 4), the $\Delta H_{PP}$ of the spectrum gradually broadened with decreasing temperature (Figure 5). Since the unpaired electron in $\mathbf{3}^+$ has the potential to be delocalized on the branched triamine moieties on the basis of the above study on $\mathbf{2}^+$, such a temperature dependency can be ascribe to the central 1,3,5-benzenetriyl moiety. It has generally been accepted that the presence of three quasi-degenerate NBMOs derived from the 1,3,5-benzenetriyl framework represents a small electronic coupling among the substituted redox-active branches.[22,23] This was also confirmed by the small potential differences between the first three oxidation processes as described in the before-mentioned electrochemical studies. We demonstrate that such a small electronic coupling results in the formation of a barrier to the thermally activated ICT via the central 1,3,5-benzenetriyl bridging unit. In other words, the delocalization of the unpaired electron in $\mathbf{3}^+$ is limited within one branched moiety, whereas the thermally activated ICT process is essential for the charge transfer among the branched three triamine moieties.

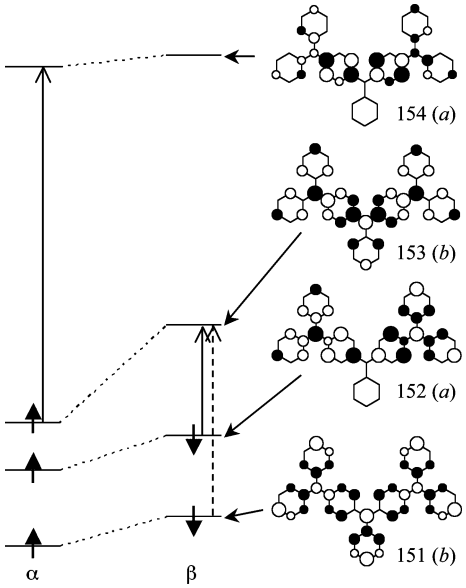


**Figure 8.** Relative energy levels of the frontier MOs for $\mathbf{2}^+$ ($C_2$ symmetry) based on the UB3LYP/3-21G* calculations. The arrows with solid and dashed lines represent the major contributions to the lowest and next-lowest energy transitions, respectively.

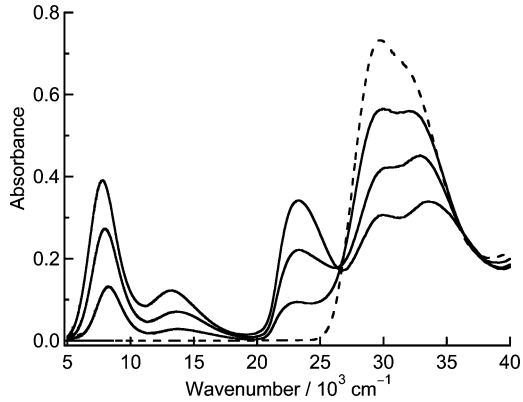


**Figure 9.** UV/vis/NIR spectra of the stepwise electrochemical oxidation of **3** in dichloromethane/0.1 M $n$-$Bu_4NBF_4$: dashed curve, neutral state; solid curve, oxidation of **3** to $\mathbf{3}^{3+}$.

The dynamics of the ICT in $\mathbf{3}^+$ was theoretically simulated by the use of the ESR-EXN program on the basis of the stochastic Liouville method.[24] On the assumption of the dynamic exchange among the three conformations where the unpaired electron is fully localized on each of the branched three triamine moieties, the simulations were carried out by using the hyperfine coupling constants determined for $\mathbf{2}^+$. The above-mentioned minor hfc constants for the 30 hydrogen nuclei were omitted and incorporated into the spectral line width. The first-order rate constants ($k_{th}$) for the thermally activated ICT were determined by comparison between the experimental and simulated ESR spectra. The resulting $k_{th}$ values gave a clear linear relationship on the basis of the Eyring plot [$\ln(k_{th}/T)$ vs $1/T$] (Figure 6). From this plot, the activation enthalpy ($\Delta H^{\ddagger}$) and entropy ($\Delta S^{\ddagger}$) for the barrier to the thermally activated ICT between two adjacent redox-active triamine branches were estimated to be 3.1 kcal mol$^{-1}$ and $-6.8$ e.u., respectively.

**Spectroelectrochemistry.** In order to confirm the presence of the IV state in $\mathbf{2}^+$ and $\mathbf{3}^+$, we need to observe the characteristic absorption band in the near-IR (NIR) region for the monocationic state on the basis of the spectroelectrochemical method. We measured the optical absorption spectral changes of **2** and **3** in DM during the course of the oxidation going from neutral to monocation $\mathbf{2}^+$ or trication $\mathbf{3}^{3+}$ by using an optically transparent thin-layer electrochemical cell.

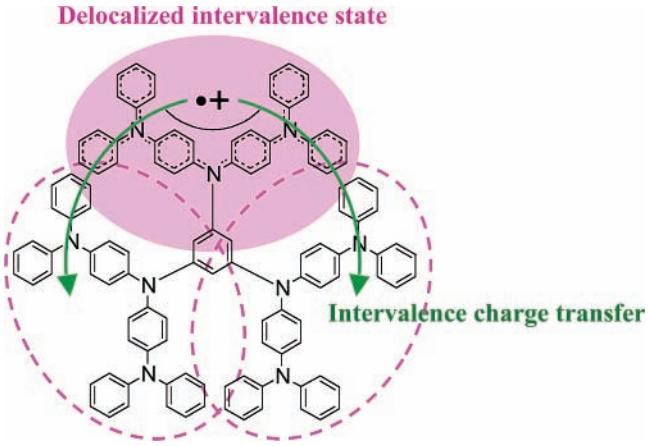


**Figure 10.** Generated charge is fully delocalized in the branched one triamine unit in $\mathbf{3}^+$ and, furthermore, can be transferred through relatively small electronic coupling between the adjacent triamine units connected by the 1,3,5-benzenetriyl bridging unit.

During the oxidation process of **2** to $\mathbf{2}^+$, new absorption bands appeared at 8117, 14350, and 23040 cm$^{-1}$ (Figure 7). This spectral pattern is quite different from that of the *para*-phenylenediamine radical cation ($\mathbf{1}^+$),[11] which is simply because the number of redox-active sites in **2** is different from that in $\mathbf{1}^+$. Delocalized IV compounds have symmetrical charge distributions, and therefore, the charge is delocalized on the bridging unit. This means that the usual quantum chemical calculations allow us to assign the low-energy absorption bands of the delocalized IV compounds to specific electronic transitions. Hence, we carried out the quantum chemical calculations based on the time-dependent density functional method (TD-DFT).[21,25] As a consequence, it was found that the TD-DFT-calculated results elucidate the observed spectrum of $\mathbf{2}^+$ (Table 2 and Figure 7). The lowest energy band is assigned to a mixture of transitions: (i) from $\beta$ (HOMO) to $\beta$ (LUMO) [72%], and (ii) from $\alpha$ (HOMO) to $\alpha$ (LUMO) [2%]. On the other hand, the next-lowest transition (14350 cm$^{-1}$) is mainly composed of the transition $\beta$ (HOMO-1) to $\beta$ (LUMO) [91%]. Moreover, the relative intensity between the lowest and next-lowest bands is well-reproduced by the calculated oscillator strengths. Therefore, we concluded that $\mathbf{2}^+$ is in a delocalized IV state.

In the spectral changes of the star-shaped nonaamine **3**, the peak positions of all newly appeared absorption bands remained unchanged during the course of oxidation to the trication $\mathbf{3}^{3+}$, and its band shape was similar to that of $\mathbf{2}^+$ (Figures 9). Furthermore, the peak intensity of $\mathbf{3}^{3+}$ was three times as large as that of $\mathbf{2}^+$. This result is consistent with the fact that the three triamines **2** are connected by the 1,3,5-benzenetriyl moiety in **3**. Hence, the lowest energy band at 7825 cm$^{-1}$ for $\mathbf{3}^{3+}$ corresponds to the IV band at 8117 cm$^{-1}$ for $\mathbf{2}^+$. This IV band is attributed to the electron delocalization within the branched triamine moiety. On the other hand, we detected no IV-CT band originating from the ICT between the adjacent redox-active triamine moieties via the 1,3,5-benzenetriyl bridging unit in the NIR region. This may be due to the spectral overlap with other intense bands.

## Conclusions

We have investigated the IV states of the monocationic states of the star-shaped nonaamine (**3**) and the triamine (**2**) as the branched unit in **3** in order to give new insight into the IV states

for the radical cations of the oligoarylamines having multiple redox-active amino groups. The charge (or spin) delocalization over the three redox-active sites in $\mathbf{2}^+$ was demonstrated by the ESR spectral simulations and the temperature-independent spectral line shape. This was also supported by the comparison of the NIR absorption spectrum of $\mathbf{2}^+$ with the TD-DFT-calculated results. On the other hand, the temperature dependency of the peak-to-peak ESR line width of $\mathbf{3}^+$ revealed that the central 1,3,5-benzenetriyl moiety leads to the thermally activated ICT process among the three branched triamine moieties. As shown in Figure 10, the coexistence of two types of the IV states in the single molecule is of great interest in connection with the possibility of dynamical control of the ICT process by the external stimuli such as thermal and electrochemical ones.

**Acknowledgment.** This work was supported by CREST (Core Research for Evolutional Science and Technology) of Japan Science and Technology Agency (JST) and by a Grant-in-Aid for Scientific Research from Japan Society for Promotion of Science (JSPS). Numerical calculations were partly carried out at the Supercomputer Laboratory of the Institute for Chemical Research of Kyoto University.

**Supporting Information Available:** Synthetic details for compounds **2** and **3**. This material is available free of charge via the Internet at http://pubs.acs.org.

## References and Notes

(1) Forrest, S. R. *Chem. Rev.* **1997**, *97*, 1793−1896.

(2) Shirota, Y. *J. Mater. Chem.* **2000**, *10*, 1−25, and references therein.

(3) (a) Wolfe, J. P.; Wagaw, S.; Buchwald, S. L. *J. Am. Chem. Soc.* **1996**, *118*, 7215−7216. (b) Marcoux, J.-F.; Wagaw, S.; Buchwald, S. L. *J. Org. Chem.* **1997**, *62*, 1568−1569. (c) Old, D. W.; Wolfe, J. P.; Buchwald, S. L. *J. Am. Chem. Soc.* **1998**, *120*, 9722−9723. (d) Wolfe, J. P.; Tomori, H.; Sadighi, J. P.; Yin, J.; Buchwald, S. L. *J. Org. Chem.* **2000**, *65*, 1158−1174. (e) Zim, D.; Buchwald, S. L. *Org. Lett.* **2003**, *5*, 2413−2415.

(4) (a) Driver, M. S.; Hartwig, J. F. *J. Am. Chem. Soc.* **1996**, *118*, 7217−7218. (b) Hamann, B. C.; Hartwig, J. F. *J. Am. Chem. Soc.* **1998**, *120*, 7369−7370. (c) Hartwig, J. F. *Angew. Chem., Int. Ed.* **1998**, *37*, 2046−2067. (d) Hartwig, J. F.; Kawatsura, M.; Hauck, S. I.; Shaughnessy, K. H.; Alcazar-Roman, L. M. *J. Org. Chem.* **1999**, *64*, 5575−5580. (e) Kataoka, N.; Shelby, Q.; Stambuli, J. P.; Hartwig, J. F. *J. Org. Chem.* **2002**, *67*, 5553−5566.

(5) (a) Nishiyama, M.; Yamamoto, T.; Koie, Y. *Tetrahedron Lett.* **1998**, *39*, 617−620. (b) Watanabe, M.; Nishiyama, M.; Yamamoto, T.; Koie, Y. *Tetrahedron Lett.* **2000**, *41*, 481−483.

(6) (a) Singer, R. A.; Sadighi, J. P.; Buchwald, S. L. *J. Am. Chem. Soc.* **1998**, *120*, 213−214. (b) Sadighi, J. P.; Singer, R. A.; Buchwald, S. L. *J. Am. Chem. Soc.* **1998**, *120*, 4960−4976. (c) Louie, J.; Hartwig, J. F. *Macromolecules* **1998**, *31*, 6737−6739. (d) Goodson, F. E.; Hauck, S. I.; Hartwig, J. F. *J. Am. Chem. Soc.* **1999**, *121*, 7527−7539. (e) Ito, A.; Taniguchi, A.; Yamabe, T.; Tanaka, K. *Org. Lett.* **1999**, *1*, 741−743. (f) Michinobu, T.; Takahashi, M.; Tsuchida, E.; Nishide, H. *Chem. Mater.* **1999**, *11*, 1969−1971. (g) Michinobu, T.; Inui, J.; Nishide, H. *Org. Lett.* **2003**, *5*, 2165−2168. (h) Murata, H.; Takahashi, M.; Namba, K.; Takahashi, N.; Nishide, H. *J. Org. Chem.* **2004**, *69*, 631−638.

(7) (a) Wienk, M. M.; Janssen, R. A. J. *J. Am. Chem. Soc.* **1997**, *119*, 4492−4501. (b) Stickley, K. R.; Selby, T. D.; Blackstock, S. C. *J. Org. Chem.* **1997**, *62*, 448−449. (c) Selby, T. D.; Blackstock, S. C. *J. Am. Chem. Soc.* **1998**, *120*, 12155−12156. (d) Selby, T. D.; Kim, K.-Y.; Blackstock, S. C. *Chem. Mater.* **2002**, *14*, 1685−1690. (e) Ranasinghe, M. I.; Varnavski, O. P.; Pawlas, J.; Hauck, S. I.; Louie, J.; Hartwig, J. F.; Goodson, T., III. *J. Am. Chem. Soc.* **2002**, *124*, 6520−6521. (f) Ito, A.; Ino, H.; Matsui, Y.; Hirao, Y.; Tanaka, K. *J. Phys. Chem. A* **2004**, *108*, 5715−5720. (g) Hirao, Y.; Ino, H.; Ito, A.; Tanaka, K.; Kato, T. *J. Phys. Chem. A* **2006**, *110*, 4866−4872.

(8) (a) Lambert, C.; Nöll, G. *Angew. Chem., Int. Ed.* **1998**, *37*, 2107−2110. (b) Lambert, C.; Nöll, G.; Hampel, F. *J. Phys. Chem. A* **2001**, *105*, 7751−7758. (c) Lambert, C.; Nöll, G. *Chem. Eur. J.* **2002**, *8*, 3467−3477. (d) Lambert, C. *ChemPhysChem* **2003**, *4*, 877−880. (e) Lambert, C.; Schelter, J.; Fiebig, T.; Mank, D.; Trifonov, A. *J. Am. Chem. Soc.* **2005**, *127*, 10600−10610.

(9) (a) Ito, A.; Ono, Y.; Tanaka, K. *J. Org. Chem.* **1999**, *64*, 8236−8241. (b) Ito, A.; Ono, Y.; Tanaka, K. *Angew. Chem., Int. Ed.* **2000**, *39*, 1072−1075. (c) Hauck, S. I.; Lakshmi, K. V.; Hartwig, J. F. *Org. Lett.* **1999**, *1*, 2057−2060. (d) Yan, X. Z.; Pawlas, J.; Goodson, T., III; Hartwig, J. F. *J. Am. Chem. Soc.* **2005**, *127*, 9105−9116.

(10) (a) Nelsen, S. F.; Ismagilov, R. F.; Powell, D. R. *J. Am. Chem. Soc.* **1996**, *118*, 6313−6314. (b) Nelsen, S. F.; Ismagilov, R. F.; Powell, D. R. *J. Am. Chem. Soc.* **1997**, *119*, 10213−10222.

(11) (a) Lambert, C.; Nöll, G. *J. Am. Chem. Soc.* **1999**, *118*, 8434−8442. (b) Lambert, C.; Nöll, G.; Schelter, J. *Nat. Mater.* **2002**, *1*, 69−73. (c) Lambert, C.; Nöll, G. *J. Chem. Soc., Perkin Trans. 2* **2002**, 2039−2043. (d) Coropceanu, V.; Lambert, C.; Nöll, G.; Brédas, J.-L. *Chem. Phys. Lett.* **2003**, *373*, 153−160. (e) Low, P. J.; Paterson, M. A. J.; Puschmann, H.; Goeta, A. E.; Howard, A. K.; Lambert, C.; Cherryman, J. C.; Tackley, D. R.; Leeming, S.; Brown, B. *Chem. Eur. J.* **2004**, *10*, 83−91. (f) Coropceanu, V.; Gruhn, N. E.; Barlow, S.; Lambert, C.; Durivage, J. C.; Bill, T. G.; Nöll, G.; Marder, S. R.; Brédas, J.-L. *J. Am. Chem. Soc.* **2004**, *126*, 2727−2731.

(12) (a) Nelsen, S. F.; Tran, H. Q.; Nagy, M. A. *J. Am. Chem. Soc.* **1998**, *120*, 298−304. (b) Nelsen, S. F.; Ismagilov, R. F.; Powell, D. R. *J. Am. Chem. Soc.* **1998**, *120*, 1924−1925. (c) Nelsen, S. F.; Ismagilov, R. F.; Teki, Y. *J. Am. Chem. Soc.* **1998**, *120*, 2200−2201. (d) Bailey, S. E.; Zink, J. I.; Nelsen, S. F. *J. Am. Chem. Soc.* **2003**, *125*, 5939−5947. (e) Lockard, J. V.; Zink, J. I.; Konradsson, A. E.; Weaver, M. N.; Nelsen, S. F. *J. Am. Chem. Soc.* **2003**, *125*, 13471−13480.

(13) Szeghalmi, A. V.; Erdmann, M.; Engel, V.; Schmitt, M.; Amthor, S.; Kriegisch, V.; Nöll, G.; Stahl, R.; Lambert, C.; Leusser, D.; Stalke, D.; Zabel, M.; Popp, J. *J. Am. Chem. Soc.* **2004**, *126*, 7834.

(14) (a) Nishiumi, T.; Nomura, Y.; Higuchi, M.; Yamamoto, K. *Chem. Phys. Lett.* **2003**, *378*, 18−23. (b) Nishiumi, T.; Nomura, Y.; Chimoto, Y.; Higuchi, M.; Yamamoto, K. *J. Phys. Chem. B* **2004**, *108*, 7992−8000.

(15) (a) Martin, R. E.; Diederich, F. *Angew. Chem., Int. Ed.* **1999**, *38*, 1350−1377. (b) Carroll, R. L.; Gorman, C. B. *Angew. Chem., Int. Ed.* **2002**, *41*, 4378−4400.

(16) (a) Dougherty, D. A. *Acc. Chem. Res.* **1991**, *24*, 88−94. (b) Iwamura, H.; Koga, N. *Acc. Chem. Res.* **1993**, *26*, 346. (c) Rajca, A. *Chem. Rev.* **1994**, *94*, 871−893. (d) Crayston, J. A.; Devine, J. N.; Walton, J. C. *Tetrahedron* **2000**, *56*, 7829−7857.

(17) Ito, A.; Taniguchi, A.; Yoshizawa, K.; Tanaka, K.; Yamabe, T. *Bull. Chem. Soc. Jpn.* **1998**, *71*, 337−343.

(18) Strohriegel, P.; Jesberger, G.; Heinze, J.; Moll, T. *Makromol. Chem.* **1992**, *193*, 909−919.

(19) Berthelot, J.; Guette, C.; Essayegh, M.; Desbene, P. L.; Basserlier, J. J. *Synth. Commun.* **1986**, *16*, 1641−1645.

(20) (a) Schwyzer, R.; Costopanagiotis, A.; Sieber, P. *Helv. Chim. Acta* **1963**, *46*, 870−889. (b) Sakai, N.; Ohfune, Y. *J. Am. Chem. Soc.* **1992**, *114*, 998−1010.

(21) To get the information on the low-lying excited state of $\mathbf{2}^+$, the hybrid HF/DF (UB3LYP) calculation was performed in the time-dependent formalism. Full geometry optimization in $C_2$ symmetry was carried out for the doublet state of $\mathbf{2}^+$ by using the 3-21G* basis set. The *Gaussian 03* program package was used for all the calculations.

(22) Rovira, C.; Ruiz-Molina, D.; Elsner, O.; Vidal-Gancedo, J.; Bonvoisin, J.; Launay, J.-P.; Veciana, J. *Chem. Eur. J.* **2001**, *7*, 240−250.

(23) (a) Bonvoisin, J.; Launay, J.-P.; van der Auweraer, M.; de Schryver, F. C. *J. Phys. Chem.* **1994**, *98*, 5052−5057, see also correction **1996**, *100*, 18006. (b) Bonvoisin, J.; Launay, J.-P.; Verbouwe, W.; van der Auweraer, M.; de Schryver, F. C. *J. Phys. Chem.* **1996**, *100*, 17079−17082.

(24) Heinzer, J. *Mol. Phys.* **1971**, *22*,167−177; *Quantum Chemistry Program Exchange* **1972**, No 209. We thank Prof. S. F. Nelsen for a copy of this program (modified by P. A. Petillo, R. F. Ismagilov).

(25) (a) Bauernschmitt, R.; Ahlrichs, R. *Chem. Phys. Lett.* **1996**, *256*, 454−464. (b) Casida, M. E.; Jamorski, C.; Casida, K. C.; Salahub, D. R. *J. Chem. Phys.* **1998**, *108*, 4439−4449. (c) Stratmann, R. E.; Scuseria, G. E.; Frisch, M. J. *J. Chem. Phys.* **1998**, *109*, 8218−8224.